Activity-dependent coordination of presynaptic release probability and postsynaptic GluR2 abundance at single synapses

Hirofumi Tokuoka*[†‡] and Yukiko Goda*[‡§]

*Medical Research Council Laboratory for Molecular Cell Biology and Cell Biology Unit, and [§]Department of Neuroscience, Physiology, and Pharmacology, University College London, Gower Street, London WC1E 6BT, United Kingdom

Edited by Charles F. Stevens, The Salk Institute for Biological Studies, La Jolla, CA, and approved August 12, 2008 (received for review June 13, 2008)

The strength of an excitatory synapse depends on both the presynaptic release probability (p_r) and the abundance of functional postsynaptic AMPA receptors. How these parameters are related or balanced at a single synapse remains unknown. By taking advantage of live fluorescence imaging in cultured hippocampal neurons where individual synapses are readily resolved, we estimate p_r by labeling presynaptic vesicles with a styryl dye, FM1-43, while concurrently measuring postsynaptic AMPA receptor abundance at the same synapse by immunolabeling surface GluR2. We find no appreciable correlation between p_r and the level of surface synaptic GluR2 under basal condition, and blocking basal neural activity has no effect on the observed lack of correlation. However, elevating network activity drives their correlation, which accompanies a decrease in mean GluR2 level. These findings provide the direct evidence that the coordination of pre- and postsynaptic parameters of synaptic strength is not intrinsically fixed but that the balance is tuned by synaptic use at individual synapses.

hippocampal culture | synaptic strength | FM1-43 | neurotransmitter release | glutamate receptor

In the classical Katz model of synaptic transmission, the weight of each synapse is determined by p_r and quantal size (q), as $p_r \times q$ (1, 2). Because q is largely governed by postsynaptic receptors, synapses have to regulate both pre- and postsynaptic mechanisms to control the overall synaptic strength. Across a population of synapses, p_r (3) and postsynaptic receptor level (4) are highly heterogeneous. Therefore, it is of fundamental importance to identify how the relationship between pre- and postsynaptic strengths at individual synapses is organized. For instance, the balance between the two could be compensative, synergistic, or random. Amongst a synapse population, compensative balance would result in relatively uniform synaptic strengths. In contrast, synergistic balance would result in a biased or skewed distribution of synaptic strengths. Thus, the manner in which pre- and postsynaptic strengths are balanced might influence dendritic processing and operation of neural networks.

Previous studies on synaptic structure and physiology suggest for a positive correlation between p_r and postsynaptic surface AMPA receptor level. For example, the number of AMPA receptors is correlated to postsynaptic density (PSD) size (5, 6), which, in turn, is matched to the presynaptic active zone length (7). Also, a larger presynaptic active zone supports a larger pool of readily releasable synaptic vesicles, resulting in higher p_r (8, 9). In further support of the view that p_r and postsynaptic surface AMPA receptor abundance are correlated, overexpression of postsynaptic proteins such as PSD-95, Shank, or GluR2 enhances AMPA receptor clustering and increases spine size, and these postsynaptic changes are, in turn, accompanied by enhanced presynaptic release (10–12). Nevertheless, beyond these reports, no studies to date have directly addressed how p_r and postsynaptic AMPA receptor level are related to each other for governing basal synaptic strength.

Here, we address this issue in cultured hippocampal neurons by using live-imaging to determine p_r and postsynaptic surface GluR2 abundance at individual synapses. We find no apparent correlation between p_r and receptor abundance in either positive or negative way under normal culture condition. However, a positive correlation emerges after imposing enhanced neural network activity. These data indicate that the coordination between pre- and postsynaptic strengths is not intrinsically fixed, but that the balance can be regulated by neural activity at individual synapses.

Results

Estimation of p_r. To estimate p_r at identified individual synapses, we took advantage of the styryl dye, FM1-43 to label recycling synaptic vesicles (3, 13, 14). Recurrent excitation during dye loading stimulation was prevented by including glutamate receptor antagonists, 6-cyano-7-nitroquinoxaline-2,3-dione (CNQX) and 2-amino-5-phosphonovaleric acid (APV) in bath solution. Two FM1-43 fluorescence parameters were obtained: (*i*) quantal FM1-43 fluorescence intensity associated with a single synaptic vesicle, q (in arbitrary fluorescence units), and (*ii*) FM1-43 fluorescence gained at an individual synapse, F, on stimulation with 30 action potentials (APs) at 1 Hz; p_r was then expressed as the number of synaptic vesicles labeled per AP, where $p_r = F/q/30$. To estimate q by optical quantal analysis, neurons were stimulated with 7 APs at 0.5 Hz (Fig. 1*A*). Fig. 1*B* shows an example of FM1-43 fluorescence image after such minimal loading. The distribution of signal intensity of FM1-43 puncta was plotted and fitted to a sum of Gaussian distributions with even spacing, in which the fluorescence corresponding to the first peak was taken as the value of q (Fig. 1*C*). We estimated quantal FM1-43 fluorescence intensity each time when we performed FM1-43 measurements of F by using the same experimental setting including solutions and culture batch. On average, q was 593 ± 18 (mean ± SEM, $n = 12$), and there was no significant difference in q values between neurons cultured at 14–15 days *in vitro* (DIV) (611 ± 20, $n = 7$) and 20–22 DIV (572 ± 34, $n = 5$; $P = 0.13$, Mann–Whitney U test), the two culture ages we used. The distribution of p_r obtained by this method was comparable to previous reports [supporting information (SI) Fig. S1 and ref. 3].

Author contributions: H.T. and Y.G. designed research; H.T. performed research; H.T. analyzed data; and H.T. and Y.G. wrote the paper.

The authors declare no conflict of interest.

This article is a PNAS Direct Submission.

[†]Present address: Graduate School of Bioscience and Biotechnology, Tokyo Institute of Technology, Yokohama 226-8501, Japan.

[‡]To whom correspondence may be addressed. E-mail: tokuoka.h.aa@m.titech.ac.jp or y.goda@ucl.ac.uk.

This article contains supporting information online at www.pnas.org/cgi/content/full/0805705105/DCSupplemental.

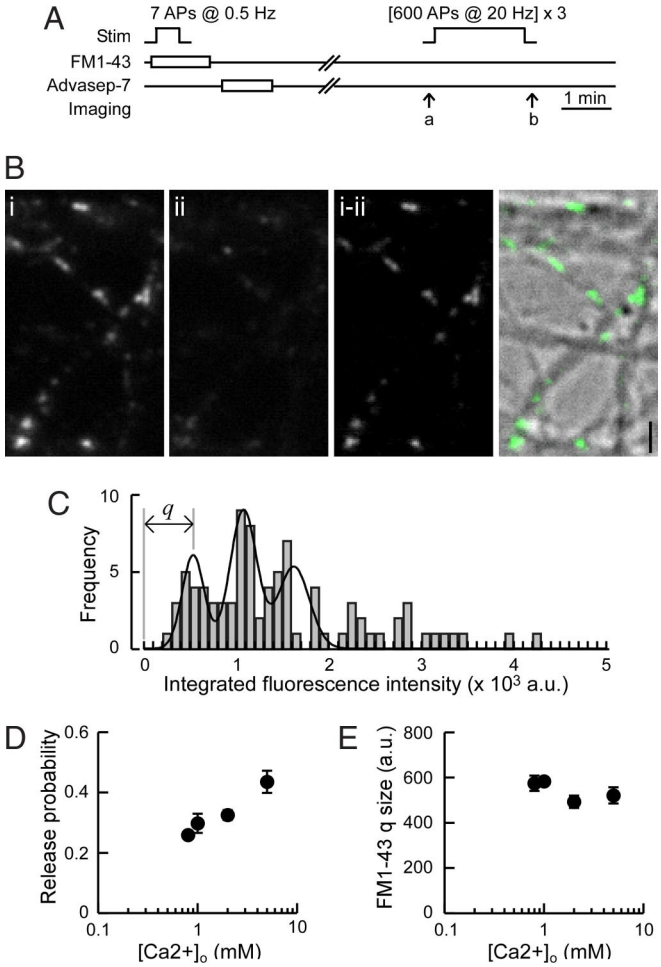

Fig. 1. Estimation of p_r by quantal analysis of FM1-43 signal. (*A*) Experimental scheme for estimating quantal FM1-43 signal from a single synaptic vesicle. FM1-43 was loaded by 7 APs at 0.5 Hz by field stimulation. After wash, FM dye was unloaded by prolonged stimulation, and the remaining signal was taken as background. Images were acquired at the time points indicated by arrows a and b. (*B*) Example images of dye-loaded synapses (*Bi*), after unloading stimulation (*Bii*), and the subtracted image (*Bi-ii*). (*Right*) Overlay of the subtracted image (*Ba-b*, green) and the differential interference contrast image. (Scale bar, 2 μm.) (*C*) Quantal analysis of FM1-43 signal from a representative experiment. The histogram was fit to the sum of three Gaussian distributions with equally spaced peaks (χ^2 test, $P = 3.5 \times 10^{-18}$). FM1-43 quantal fluorescence, *q*, for this example was 543 (a.u.). (*D*) Effect of changing $[Ca^{2+}]_o$ on p_r. FM1-43 was loaded by 7 APs at 0.5 Hz in extracellular solution containing 0.8 ($n = 3$ coverslips), 1.0 ($n = 3$), 2.0 ($n = 5$), and 5.0 mM Ca^{2+} ($n = 3$). Estimated p_r changed positively with increasing $[Ca^{2+}]_o$ ($r = 0.81$, $P = 0.0005$, Spearman rank correlation). (*E*) Effect of changing $[Ca^{2+}]_o$ on FM1-43 quantal fluorescence. There was no significant difference in *q* measured at different $[Ca^{2+}]_o$ ($P > 0.1$, Spearman rank correlation).

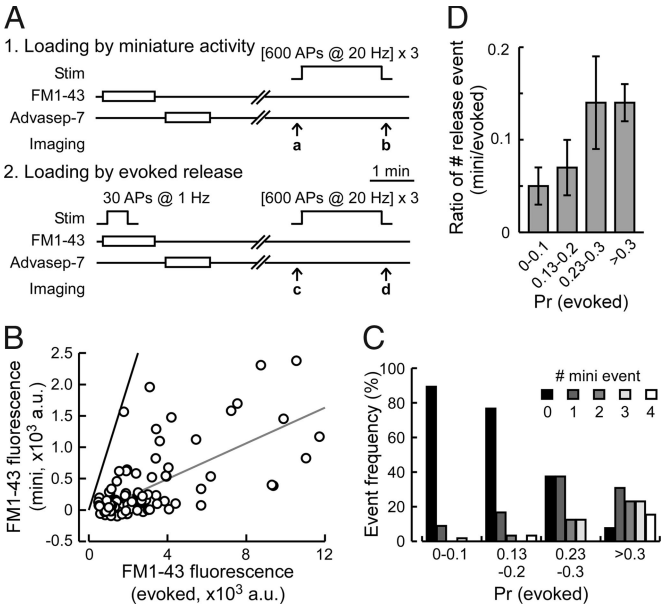

Fig. 2. Background miniature activity does not significantly affect the estimation of p_r by FM1-43. (*A*) Experimental scheme for comparing miniature spontaneous activity and evoked release. In the first session, FM1-43 was loaded by spontaneous activity, whereas in the second session FM1-43 was loaded by 30 APs at 1 Hz. Fluorescence signals from spontaneous miniature and evoked events were obtained by subtracting the unloaded image: a–b (spontaneous activity) or c–d (evoked response). (*B*) Scatter plot showing FM1-43 fluorescence intensities loaded by field stimulation (evoked) and spontaneous miniature activity (mini). The gray line is a linear regression fit with a slope of 0.142, and the black line has a slope of 1. Data from 107 regions of interest from three coverslips are shown. (*C*) Synapses are classified by their p_r, and the distribution of the miniature endocytotic event frequency is shown for each group. FM1-43 fluorescence intensity shown in *B* is converted to p_r for evoked events. Higher p_r synapses tend to show higher miniature synaptic activity ($r = 0.65$, $P < 0.0001$, Spearman correlation), although the overall contribution of miniature activity is small. (*D*) Ratio of the number of miniature release events to that of evoked release at individual synapses as a function of p_r (evoked). On average, the uptake of FM1-43 by miniature synaptic activity contributes to ≈7% of our estimation of p_r. Data are shown as mean ± SEM.

To compare p_r across many synapses, it was critical to have a sufficiently sensitive method for detecting the possible differences. We tested this point by examining the effect of varying extracellular Ca^{2+} concentration ($[Ca^{2+}]_o$) to deliberately change p_r at individual boutons. We loaded FM1-43 by 7 APs in various $[Ca^{2+}]_o$ ranging from 0.8 to 5 mM; p_r increased from 0.26 to 0.44 in parallel with $[Ca^{2+}]_o$ increase (Fig. 1*D*). Importantly, the quantal FM1-43 fluorescence signal did not significantly change as a function of $[Ca^{2+}]_o$ (Fig. 1*E*). Thus, our quantal analysis of FM1-43 fluorescence was sensitive enough to detect approximately a two-fold range in p_r associated with different $[Ca^{2+}]_o$.

Of the two parameters for calculating p_r, *F* was obtained by FM1-43 loading protocol of 30 APs at 1 Hz, and the dye was left in the external bath solution for an additional 30 s after the AP train to allow for compensative endocytosis that occurs within ≈30 s (15). This protocol induced repetitive release with little presynaptic short-term plasticity (ref. 16 and data not shown), thus enabling for an estimate of basal p_r. Whereas recurrent AP firing was blocked by CNQX and APV, synaptic vesicles could undergo spontaneous release and endocytosis during the period of FM1-43 loading. We tested if such spontaneous release events contributed to our estimation of p_r. We compared the extent FM1-43 loading of vesicles between our standard AP-triggered (evoked) protocol and with spontaneous activity alone for the same duration (70 s) (Fig. 2 *A* and *B*). As reported previously (17), p_r and spontaneous event frequency were positively correlated (Spearman rank correlation, $r = 0.65$, $P < 0.0001$; Fig. 2*C*), confirming that high p_r synapses show more frequent spontaneous release events. However, the average spontaneous release event constituted a small proportion of the evoked release (7.4 ± 1.5%; Fig. 2*D*), and majority of synapses (77 out of 107) displayed no spontaneous release events during the FM1-43 loading period. Therefore, spontaneous release has negligible or very minor impact on our estimation of p_r.

Preferential Expression of GluR2 in Spiny Neurons. To quantify the abundance of surface AMPA receptors at the synapse, we

monitored GluR2, the predominant AMPA receptor subunit at mature synapses in hippocampal cultures (18). We reasoned that, in contrast to the GluR1 subunit that forms Ca^{2+}-permeable AMPA receptors and whose surface expression is highly regulated by activity in hippocampal neurons, GluR2 surface levels might more closely represent constitutive postsynaptic strength (19, 20). Surface GluR2 was live-labeled by using an antibody against the extracellular epitope of GluR2 (21); previous reports had indicated that antibodies could penetrate the native synaptic cleft (22, 23). The GluR2 labeling showed clear, discrete fluorescence puncta that colocalized with an excitatory postsynaptic marker, PSD-95 (Fig. S2*E*). We noticed that some neurons did not express detectable level of GluR2. To characterize these neurons, we randomly expressed CFP to correlate neuronal morphology with GluR2 labeling. We found that almost all GluR2-expressing neurons were spiny (10 out of 10 cells; Fig. S2 *A* and *B*), whereas GluR2-lacking neurons were either spiny or aspiny (four spiny and three aspiny out of seven cells; Fig. S2 *C* and *D*). In contrast, GluR1 was expressed in most neurons (data not shown). Because the principal pyramidal neurons are spiny, whereas most interneurons are aspiny in the hippocampus, by examining GluR2 expression we have limited our study to putative pyramidal neurons.

Concurrent Estimation of p_r and Surface GluR2 Level at Single Synapses. We next combined p_r estimation by using FM1-43 with live-labeling of surface GluR2. Living cultured neurons were incubated with anti-GluR2 antibody for 15 min, followed by Alexa594-conjugated secondary antibody for a further 15 min. Neurons were then subjected to FM1-43 labeling protocol (30 AP at 1 Hz), as described above to load recycling vesicles. Fig. 3*A* shows an example overlay image of FM1-43 and GluR2 signals. For the analysis we chose all pairs of overlapping FM1-43 and GluR2 puncta that were well isolated from others (Fig. 3 *B* and *C*), and the relationship between p_r and GluR2 level was examined by scatter plots (Fig. 3 *D*–*G*). At 14–15 DIV, after a period of robust synaptogenesis when synapses were fully functional, we did not find any apparent correlation between the two parameters (Fig. 3 *D* and *F*). To test if such a lack of correlation reflected some aspect of developmental immaturity, we examined the relationship in older cultures at 20–22 DIV. We again did not see an obvious correlation between p_r and postsynaptic GluR2 level (Fig. 3 *E* and *G*). These data suggest that under normal culture condition, pre- and postsynaptic strengths are not coordinated, despite the presence of spontaneous activity that triggers synaptic communication between pre- and postsynaptic terminals.

Enhancing Neural Excitability Increases the Correlation Between p_r and Postsynaptic GluR2 Level. Our finding that p_r and postsynaptic receptor abundance were not correlated under basal condition raised a possibility that the balance between the two could be regulated by changes in network activity. To examine this point, we tested the effect of elevating activity by increasing the extracellular KCl concentration by 5 mM while blocking inhibitory inputs with 10 μM bicuculline, a $GABA_A$ receptor antagonist. After enhanced activity treatment for 2 days (48 to 54 h), p_r and GluR2 level were correlated in both 14–15 DIV and 20–22 DIV neurons (Fig. 4 *A* and *B*). Comparison with control nontreated cultures indicated that the correlation was attributable to the preferential down-regulation of GluR2 at low p_r synapses. Whereas the KCl/bicuculline treatment did not measurably alter the distribution of p_r, the overall surface GluR2 level was decreased (Fig. 4 *C*–*F* and Fig. S3), which was consistent with synaptic scaling of AMPA receptors as reported previously (24). The lack of an apparent change in p_r is likely due to the mild activity-enhancing condition used in the present study (25). These data suggest that an increase in network activity and the resulting increased synaptic usage promotes the coordination of p_r and postsynaptic GluR2 level. The correlation increased to similar extents in both 14–15 DIV and 20–22 DIV cultures. Therefore, coordination of pre- and postsynaptic strengths likely occurs by modulating existing synapses rather than involving synapse formation, because younger cultures with a higher capacity for synapse formation does not show a preferential increase in correlation.

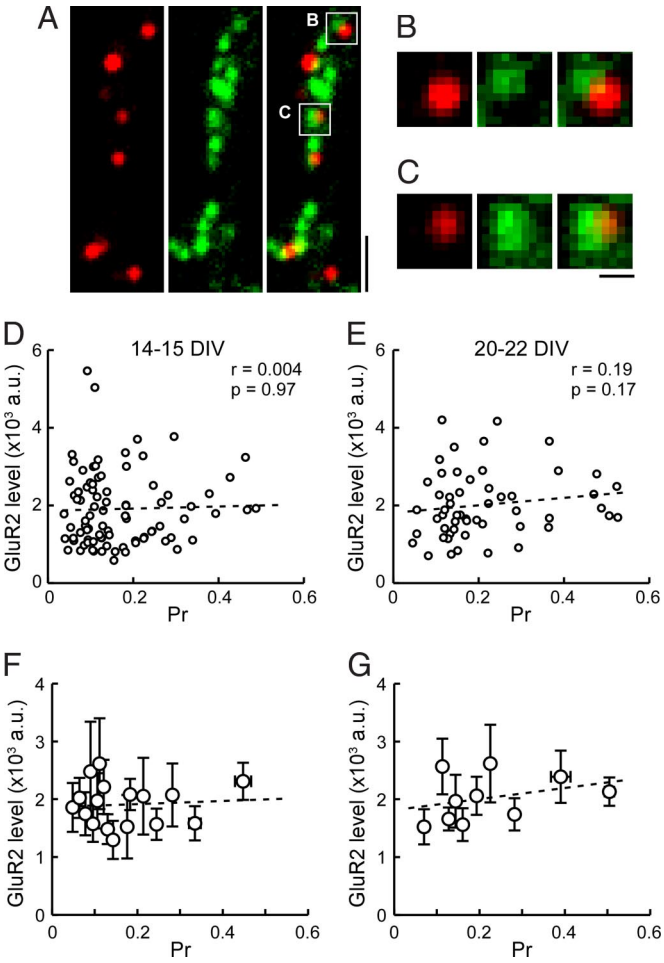

Fig. 3. Dual imaging of p_r and postsynaptic GluR2 level. (*A*) Example field of view showing surface GluR2 labeling (red, *Left*), presynaptic FM1-43 signal (green, *Center*), and merge (*Right*). Cultured neurons were first live-labeled with anti-GluR2 antibody, and subjected to FM1-43 experiment to examine p_r. FM1-43 was loaded by 30 APs at 1 Hz. (Scale bar, 2 μm.) (*B* and *C*) Examples of synaptic areas boxed in *A*, where FM1-43 and GluR2 signals overlap. Only synapses harboring a single FM1-43 punctum apposed by a single GluR2 punctum were chosen for analysis. (Scale bar, 0.5 μm.) (*D* and *E*) Scatter plots of p_r and GluR2 fluorescence intensities at individual synapses from 14–15 DIV (*D*, $n = 88$ boutons, five coverslips) and 20–22 DIV neurons (*E*, $n = 54$ boutons, five coverslips). Correlation coefficient (r) and *P* value (p) by Spearman rank correlation test are shown. No apparent correlation is observed for both culture groups. (*F* and *G*) Summary plots of GluR2 level versus p_r from *D* and *E*. Each point represents an average of five or six synapses, grouped in the order of p_r. Error bars indicate ± SEM. Dotted lines are linear regression fits.

Effect of Activity Blockade on the Relationship Between p_r and Postsynaptic GluR2 Level. Whereas enhanced activity drove the coordination of pre- and postsynaptic strengths, we did not observe an appreciable correlation under basal condition when neurons showed spontaneous spiking. To examine the contribution, if any, of basal spontaneous excitatory activity in matching of p_r and GluR2 abundance, we treated neurons with 10 μM

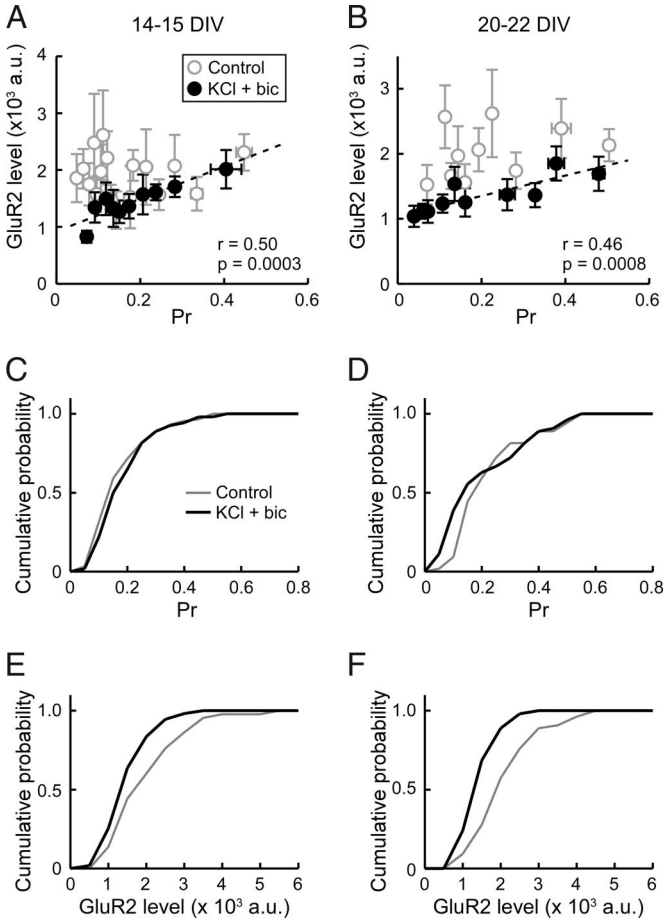

Fig. 4. Effect of enhancing neural excitability on the correlation between p_r and postsynaptic GluR2 fluorescence level. (*A* and *B*) Summary of GluR2 level versus p_r relationship from 14–15 DIV neurons (*A*, $n = 61$ boutons, five coverslips) and 20–22 DIV neurons (*B*, $n = 54$ boutons, five coverslips) treated with 5 mM KCl and 10 μM bicuculline for 2 days (filled circles). Each point represents an average from five to six boutons. Dotted lines are linear regression fits. Data from the control experiment is also shown (open circles). Correlation coefficient (r) and *P* value (p) by Spearman rank correlation test are indicated. At both culture ages, treatment with KCl and bicuculline significantly increases the correlation between p_r and GluR2 level. (*C* and *D*) Cumulative distribution plots of p_r at 14–15 DIV (*C*) and 20–22 DIV (*D*). (*E* and *F*) Cumulative distribution plots of GluR2 level at 14–15 DIV (*E*) and 20–22 DIV (*F*). Treatment with KCl and bicuculline decreased GluR2 level. K-S test, $P = 0.0136$ (14–15 DIV), $P = 0.0002$ (20–22 DIV).

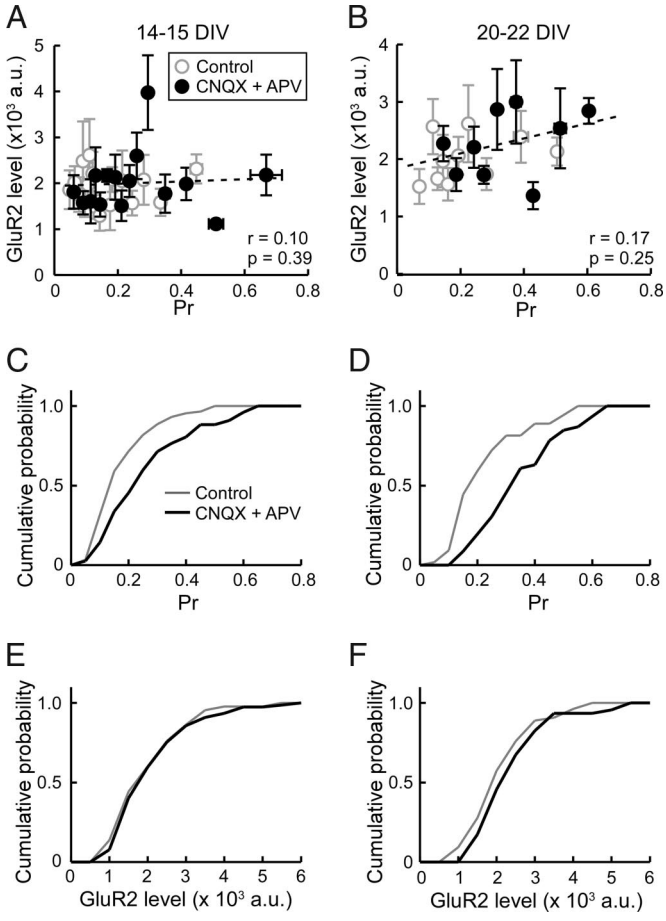

Fig. 5. Effect of blocking excitatory synaptic transmission on the correlation between p_r and postsynaptic GluR2 level. (*A* and *B*) Summary of GluR2 level versus p_r relationship from 14–15 DIV neurons (*A*, $n = 77$ boutons, six coverslips) and 20–22 DIV neurons (*B*, $n = 46$ boutons, three coverslips) treated with or without CNQX (10 μM) and APV (50 μM) for 2 days (filled circles). Each point is an average from five to six boutons. Dotted lines are linear regression fits. Data from the control experiment is also shown (open circles). Correlation coefficient (r) and p value (p) by Spearman rank correlation test are indicated. Treatment with CNQX and APV does not produce a significant correlation between p_r and GluR2 level. (*C* and *D*) Cumulative distribution plots of p_r at 14–15 DIV (*C*) and 20–22 DIV (*D*). Treatment with CNQX and APV increased p_r. K-S test, $P = 0.0058$ (14–15 DIV), $P < 0.0001$ (20–22 DIV). (*E* and *F*) Cumulative distribution plots of GluR2 level at 14–15 DIV (*E*) and 20–22 DIV (*F*).

CNQX and 50 μM APV for 2 days before FM1-43 and GluR2 imaging. After complete blockade of excitatory transmission, p_r was significantly increased (Fig. 5 *C* and *D* and Fig. S3), as previously reported (26). However, the relationship between p_r and GluR2 level remained uncorrelated at both 14–15 DIV and 20–22 DIV (Fig. 5 *A* and *B*). We also examined the effect of tetrodotoxin (TTX), a sodium channel blocker, to inhibit spontaneous spikes. Again, the relationship between p_r and GluR2 level was not significantly altered after 2 days of activity suppression (Fig. S3 and Fig. S4). Therefore, it is unlikely that an intrinsic, activity-independent mechanism coordinates p_r and surface GluR2 level.

Discussion

Synaptic strength is governed by both p_r and the number of functional postsynaptic receptors. It has not been easy to quantify both parameters at the level of single synapses. Whereas electrophysiology offers high sensitivity and great temporal resolution, recording evoked synaptic responses from a single bouton containing a single release site is technically challenging. Electron microscopy is another possible technique, although it is very laborious to concurrently measure p_r (e.g., by FM1-43 photoconversion) and postsynaptic receptor abundance (e.g., by immuno-gold labeling) from large population of synapses. To overcome these difficulties, we combined two fluorescence live-imaging techniques: measurements of p_r, by using FM1-43 (3, 13, 14), and live-labeling of postsynaptic surface GluR2 receptors (20, 21). We found that p_r and postsynaptic surface GluR2 abundance are not appreciably correlated under basal culture condition. However, enhancing activity by raising extracellular K^+ and silencing GABAergic inputs resulted in their correlation. Our data provides the direct evidence that p_r and postsynaptic AMPAR abundance are not necessarily correlated by an intrinsic mechanism as synaptic contacts are formed, but neural activity drives their correlation at single synapses.

FM1-43 is a useful tool to study synaptic vesicle recycling (27, 28), enabling the tracking of single synaptic vesicle dynamics (3,

13, 14). Despite its established usefulness, FM1-43 imaging poses potential technical limitations for estimating p_r. Such limitations could arise from the dependence on an indirect, compensatory endocytosis for FM1-43 loading of vesicles, and the relatively high background fluorescence attributable to the lipophilic nature of the styryl dye. Our method was sufficiently sensitive for detecting variable p_r on altering extracellular Ca^{2+}, at least approximately a two-fold range. This range was narrower than that predicted by previous studies of Ca^{2+}-dependence of neurotransmitter release examined by whole-cell patch clamp recordings in cultured hippocampal neurons (29, 30), and thus, our ability to detect very low p_r synapses with low signal-to-noise may have been compromised. Nevertheless, activity-induced correlation between p_r and GluR2 abundance occurred by the preferential loss of GluR2 at low p_r synapses. This observation suggested that low p_r synapses as identified by our measure were not inherently noisy and did not necessarily mask the possible correlation under control conditions. The contribution from spontaneously recycling synaptic vesicles that could bias the measurements of p_r was also minimal under our experimental conditions.

Another technique we used was live-labeling of surface GluR2 receptors. We reasoned that GluR2 might be a suitable indicator of postsynaptic strength, because excitatory synaptic currents in glutamatergic hippocampal neurons are primarily mediated by GluR2-containing AMPA receptors, whereas GluR2-lacking AMPA receptors are suggested to be recruited transiently in the process of postsynaptic plasticity (19, 20). As an added advantage, selecting GluR2-positive neurons that were mostly spiny, a feature shared by most pyramidal neurons in hippocampal CA3 to CA1 regions, allowed sampling of data from a relatively uniform population of neurons rather than from mixed neuronal types present in the culture. During the 30-min incubation with the primary and secondary antibodies, certain amount of GluR2 may undergo endocytosis (31) or lateral diffusion to nonsynaptic sites (32), thereby escaping their detection at the synaptic surface. Thus, our estimate of the receptor abundance is likely to provide a lower limit, although the turnover of basal AMPA receptors is slow, with $<10\%$ of the receptors being endocytosed in 10 min. Additional source of error in the GluR2 measurements concerns the accessibility of the antibody for synaptic GluR2. Whereas the synaptic cleft ($\approx$20 nm) is of comparable size to the IgG ($\approx$15 nm in the maximum dimension), antibodies have been shown to penetrate the synaptic cleft in live preparations (22, 23). Also, a recent *in vivo* study has suggested that synaptic cleft sizes can be at least two fold wider than the previous estimates based on ultrastructural analysis of fixed tissue (33). Whereas synaptic junctions may appear stable, their adhesive state could be dynamic in living neurons (34, 35), permitting the passage of IgG, which has flexible hinge regions. Importantly, GluR2 labeling colocalized with PSD-95 signals, and showed clear, distinct punctae that neatly apposed the presynaptic FM1-43 signal. Thus, most extracellularly labeled GluR2 signals represented synaptic receptors, thereby validating our method for assessing postsynaptic GluR2 level.

Our finding of a lack of correlation between p_r and the GluR2 abundance was somewhat unexpected. Previous observations have led to the popular assumption that p_r and postsynaptic potency are matched (see above), such that high p_r synapses have a higher number of receptors compared with low p_r synapses. Whereas these studies may have involved synapses that have already experienced substantial activity, a condition we have found to enhance the correlation, our overall findings are in agreement with other previous reports suggesting that p_r may not necessarily correlate with postsynaptic receptor number. For example, BDNF increases active zone size but not quantal amplitude (36), showing the dissociation between regulation of active zone size and functional synaptic AMPA receptor abundance. Mismatch of active zone size and PSD size can also occur *in vivo*, as seen on conditional ablation of delta2 glutamate receptor gene in the adult mouse cerebellum (37). Therefore, the relationship between active zone and PSD size or AMPA receptor abundance are not always stereotypically fixed and there are mechanisms that differentially set these parameters.

Neural activity can modulate the structure and function of both the pre- and the postsynaptic terminals in many ways. Here, we find that the enhancement of network activity drives the coordination of pre- and postsynaptic strengths, resulting in emergence of their correlation. Candidate underlying mechanism could involve synaptic adhesion proteins that link the pre- and postsynaptic terminals and organize presynaptic vesicle clusters (38) and postsynaptic AMPA receptors (39, 40) in an activity-dependent manner (38, 39). Notably, a postsynaptic complex of neuroligin, the binding partner of presynaptic neurexin, and PSD-95, a postsynaptic scaffold protein, can retrogradely regulate p_r (41). Therefore, adhesion protein complexes display features expected of a machinery that fine-tunes the balance of pre- and postsynaptic strengths according to the level of activity that the synapse experiences. Interestingly, when the correlation between pre- and postsynaptic strengths was promoted by activity enhancement, the mean GluR2 abundance was reduced but the mean p_r was not significantly changed in the present experimental condition. This observation may perhaps imply that the modification of postsynaptic strength is more responsive in such activity-dependent coordination of pre- and postsynapse.

We found that spontaneous activity in the basal culture condition was not sufficient to drive the pre- and postsynaptic correlation. This result may be because spontaneous activity was not sufficiently strong or patterned, at least in our dissociated cultures. It would be of interest to examine how such coordination is organized *in vivo*, where physiological spontaneous activity shapes the pattern of synaptic connections during development. Our data show that low p_r synapses are most affected by the increased activity, where their GluR2 level is reduced. Such a change may share mechanisms with activity-dependent pruning or elimination of excess synapses that occur in developing neurons.

Methods

Cell Culture. Dissociated cultures of hippocampal CA1-CA3 neurons were prepared from P0 rats as described previously with minor modifications (16, 28). In some experiments, cells were treated with TTX (1 μM), CNQX (10 μM) + APV (50 μM), or KCl (5 mM) + bicuculline (10 μM) for 2 days before FM1-43 experiments. Neurons were used for experiments at 14–15 and at 20–22 DIV. Animal care and use were approved by the U.K. Home Office. For details, see *SI Methods*.

Live-Labeling of GluR2. Neurons were first labeled with 5 μg/ml anti-GluR2 monoclonal antibody (MAB397, Chemicon) in culture medium for 15 min. After a brief wash, secondary labeling with 5 μg/ml Alexa594-conjugated anti-mouse IgG antibody (Invitrogen) was for an additional 15 min in culture medium. Coverslips were then immediately used for FM1-43 experiments. For details, see *SI Methods*.

FM1-43 Experiment. Basic set up for FM1-43 experiments was as described previously (28). Neurons were loaded with FM1-43 (10 μM, Invitrogen) by 7 or 30 APs evoked by 2 ms, 20 V square pulses; 30 s after the end of stimulation, excess dye was washed with EBS containing 1 mM Advasep-7 (Biotium) for 1 min, then with EBS with 0.1 mM Ca^{2+} for 5 to 10 min. After replacing with normal EBS (2 mM Ca^{2+}), images were acquired before and after unloading stimulation by 600 APs at 20 Hz for three rounds with 15-s intervals. The remaining signals were taken as background. For details, see *SI Methods*.

Image Analysis. Images were analyzed with NIH ImageJ. To quantify FM1-43 fluorescence, background signals were subtracted, and total fluorescence intensities of each puncta were measured. Fitting of FM1-43 signal to sum of three or five Gaussian distributions with even spacing was performed by Igor

Pro (WaveMetrics) by using the following equation as reported previously (3, 12, 13):

$$\sum_{i=1}^{n} A_i \exp(-(x - iq)^2/2(\sigma_0^2 + i\sigma_v^2)$$

A_i is the amplitude of ith peak, x is integrated fluorescence intensity, q is the quantal fluorescence of FM1-43 signal, and σ_0 is the variance of fluorescence of background, σ_v is the variance of fluorescence of FM1-43 signal from single vesicle. To estimate q, FM1-43 was loaded by 7 AP at 0.5 Hz.

For the measurement of p_r, FM1-43 was loaded by 30 APs at 1 Hz. After subtracting background, p_r was estimated by $p_r = F/q/30$, where F was integrated fluorescence intensity of a FM1-43 punctum, and q was quantal FM1-43 fluorescence measured from other independent coverslips on the same day. When the effect of changing $[Ca^{2+}]_o$ was examined, FM1-43 was loaded by 7 APs at 0.5 Hz.

To quantify GluR2 signals, background (nonpunctate region) was subtracted, and total fluorescence intensities of each puncta were measured. We restricted our analysis to synapses with partially or completely overlapping pairs of presynaptic FM1-43 punctum and postsynaptic GluR2 punctum. Puncta contacting multiple partners were discarded.

Statistics. Spearman rank correlation with tie correction, Steel's multiple-comparison test, Kolmogorov–Smirnov (K-S) test, and Mann–Whitney U test were used as required. P value of <0.05 was taken as significant. Data are shown as mean ± SEM unless otherwise noted.

ACKNOWLEDGMENTS. We thank Y.G. laboratory members for help and discussion, and T. Branco, L. Cingolani, and N. Vitureira for critical comments on the manuscript. H.T. was supported by a postdoctoral fellowship for research abroad from the Japan Society for the Promotion of Science. This work was supported by the Medical Research Council and the European Commission Framework VI (EUSynapse project, LSHM-CT-2005-019055).

1. Del Castillo J, Katz B (1954) Quantal components of the end-plate potential. *J Physiol* 124:560–573.
2. Del Castillo J, Katz B (1954) Statistical factors involved in neuromuscular facilitation and depression. *J Physiol* 124:574–585.
3. Murthy VN, Sejnowski TJ, Stevens CF (1997) Heterogeneous release properties of visualized individual hippocampal synapses. *Neuron* 18:599–612.
4. Matsuzaki M, *et al.* (2001) Dendritic spine geometry is critical for AMPA receptor expression in hippocampal CA1 pyramidal neurons. *Nat Neurosci* 4:1086–1092.
5. Takumi Y, Ramirez-Leon V, Laake P, Rinvik E, Ottersen OP (1999) Different modes of expression of AMPA and NMDA receptors in hippocampal synapses. *Nat Neurosci* 2:618–624.
6. Tanaka J, *et al.* (2005) Number and density of AMPA receptors in single synapses in immature cerebellum. *J Neurosci* 25:799–807.
7. Schikorski T, Stevens CF (2001) Morphological correlates of functionally defined synaptic vesicle populations. *Nat Neurosci* 4:391–395.
8. Rosenmund C, Stevens CF (1996) Definition of the readily releasable pool of vesicles at hippocampal synapses. *Neuron* 16:1197–1207.
9. Dobrunz LE, Stevens CF (1997) Heterogeneity of release probability, facilitation, and depletion at central synapses. *Neuron* 18:995–1008.
10. El-Husseini AE, Schnell E, Chetkovich DM, Nicoll RA, Bredt DS (2000) PSD-95 involvement in maturation of excitatory synapses. *Science* 290:1364–1368.
11. Sala C, *et al.* (2001) Regulation of dendritic spine morphology and synaptic function by Shank and Homer. *Neuron* 31:115–130.
12. Passafaro M, Nakagawa T, Sala C, Sheng M (2003) Induction of dendritic spines by an extracellular domain of AMPA receptor subunit GluR2. *Nature* 424:677–681.
13. Ryan TA, Reuter H, Smith SJ (1997) Optical detection of a quantal presynaptic membrane turnover. *Nature* 388:478–482.
14. Aravanis AM, Pyle JL, Tsien RW (2003) Single synaptic vesicles fusing transiently and successively without loss of identity. *Nature* 423:643–647.
15. Balaji J, Ryan TA (2007) Single-vesicle imaging reveals that synaptic vesicle exocytosis and endocytosis are coupled by a single stochastic mode. *Proc Natil Acad Sci USA* 104:20576–20581.
16. Morales M, Colicos MA, Goda Y (2000) Actin-dependent regulation of neurotransmitter release at central synapses. *Neuron* 27:539–550.
17. Prange O, Murphy TH (1999) Correlation of miniature synaptic activity and evoked release probability in cultures of cortical neurons. *J Neurosci* 19:6427–6438.
18. Pickard L, Noël J, Henley JM, Collingridge GL, Molnar E (2000) Developmental changes in synaptic AMPA and NMDA receptor distribution and AMPA receptor subunit composition in living hippocampal neurons. *J Neurosci* 20:7922–7931.
19. Plant K, *et al.* (2006) Transient incorporation of native GluR2-lacking AMPA receptors during hippocampal long-term potentiaon. *Nat Neurosci* 9:602–604.
20. Sutton MA, *et al.* (2006) Miniature neurotransmission stabilizes synaptoic function via tonic suppression of local dendritic protein synthesis. *Cell* 125:785–799.
21. Patrick GN, Bingol B, Weld HA, Schuman EM (2003) Ubiquitin-mediated proteasome activity is required for agonist-induced endocytosis of GluRs. *Curr Biol* 13:2073–2081.
22. Dahan M, *et al.* (2003) Diffusion dynamics of glycine receptors revealed by single-quantum dot tracking. *Science* 302:442–445.
23. Tardin C, Cognet L, Bats C, Lounis B, Choquet D (2003) Direct imaging of lateral movements of AMPA receptors inside synapses. *EMBO J* 22:4656–4665.
24. Turrigiano GG, Leslie KR, Desai NS, Rutherford LC, Nelson SB (1998) Activity-dependent scaling of quantal amplitude in neocortical neurons. *Nature* 391:892–896.
25. Branco T, Staras K, Darcy KJ, Goda Y (2008) Local dendritic activity sets release probability at hippocampal synapses. *Neuron* 59:475–485.
26. Murthy VN, Schikorski T, Stevens CF, Zhu Y (2001) Inactivity produces increases in neurotransmitter release and synapse size. *Neuron* 32:673–682.
27. Betz WJ, Bewick GS (1992) Optical analysis of synaptic vesicle recycling at the frog neuromuscular junction. *Science* 255:200–203.
28. Tokuoka H, Goda Y (2006) Myosin light chain kinase is not a regulator of synaptic vesicle trafficking during repetitive exocytosis in cultured hippocampal neurons. *J Neurosci* 26:11606–11614.
29. Goda Y, Stevens CF (1994) Two components of transmitter release at a central synapse. *Proc Natl Acad Sci USA* 91:12942–12946.
30. Fernández-Chacón R, *et al.* (2001) Synaptotagmin I functions as a calcium regulator of release probability. *Nature* 410:41–49.
31. Shepherd JD, Huganir RL (2007) The cell biology of synaptic plasticity: AMPA receptor trafficking. *Annu Rev Cell Dev Biol* 23:613–643.
32. Groc L, Choquet D (2006) AMPA and NMDA glutamate receptor trafficking: Multiple roads for reaching and leaving the synapse. *Cell Tissue Res* 326:423–438.
33. Thorne RG, Nicholson C (2005) In vivo diffusion analysis with quantum dots and dextrans predicts the width of brain extracellular space. *Proc Natl Acad Sci USA* 103:5567–5572.
34. Colicos MA, Collins BE, Sailor MJ, Goda Y (2001) Remodeling of synaptic actin induced by photoconductive stimulation. *Cell* 107:605–616.
35. Tai CY, Mysore SP, Chiu C, Schuman EM (2007) Activity-regulated N-cadherin endocytosis. *Neuron* 54:771–785.
36. Tyler WJ, Pozzo-Miller LD (2001) BDNF Enhances Quantal Neurotransmitter Release and Increases the Number of Docked Vesicles at the Active Zones of Hippocampal Excitatory Synapses. *J Neurosci* 21:4249–4258.
37. Takeuchi T, *et al.* (2005) Control of synaptic connection by glutamate receptor delta2 in the adult cerebellum. *J Neurosci* 25:2146–2156.
38. Bamji SX, *et al.* (2003) Role of beta-catenin in synaptic vesicle localization and presynaptic assembly. *Neuron* 40:719–731.
39. Okuda T, Yu LM, Cingolani LA, Kemler R, Goda Y (2007) Beta-Catenin regulates excitatory postsynaptic strength at hippocampal synapses. *Proc Natl Acad Sci USA* 104:13479–13484.
40. Saglietti L, *et al.* (2007) Extracellular interactions between GluR2 and N-cadherin in spine regulation. *Neuron* 54:461–477.
41. Futai K, *et al.* (2007) Retrograde modulation of presynaptic release probability through signaling mediated by PSD-95-neuroligin. *Nat Neurosci* 10:186–195.